Investigation of excitation energy dependence of fission modes in actinides through transfer-induced fission

H. Lee[1,*], *K*. *J*. Cook[1], *J*. Buete[1], *D*. *J*. Hinde[1], *M*. Dasgupta[1], *L*. *T*. Bezzina[1,**], *S*. *L*. Hayles[1], *M*. *K*. Lakelin[1], *C*. *C*. Seabra[1], *T*. Tran[1], and *M*. *M*. Webber[1]

[1]Department of Nuclear Physics and Accelerator Applications, Research School of Physics, The Australian National University, Canberra 2601, Australia

Abstract. Nuclear fission outcomes are strongly driven by different shell-stabilized fission modes. The resulting fission fragment properties sensitively depend on the excitation energy and the fissioning nuclide. To directly observe how they depend on the excitation energy of the fissioning nucleus, (d,p) transfer-induced fission of ^{233}Th has been measured at the Australian National University. The excitation-energy dependence of the reconstructed fragment mass distributions reveals a systematic evolution of the fission modes, with distinct thresholds for the onset of asymmetric and symmetric fission, and for the emergence of multi-chance fission.

1 Introduction

In nuclear fission, a heavy nucleus decays into two smaller fragments due to the competition between the repulsive Coulomb force and the attractive strong nuclear force. Fission remains one of the most complex processes in nuclear physics. The many-body quantum nature of the nucleus gives rise to structures in the distribution of fission products, reflecting the microscopic shell effects at particular nucleon numbers that stabilize the nascent fragments [1–3].

Distributions of fission fragments have been extensively studied in the actinide region, where a well-established competition exists between a mass-symmetric and two mass-asymmetric (standard I and II, at $Z \approx 52.5, 55$) modes of fission [2–5]. The evolution of these distributions with excitation energy of the fissioning system [6] remains a significant challenge for theoretical descriptions of the fission process.

The nuclear fission process can be described by the nuclear shape evolving along a trajectory on a multidimensional potential energy surface (PES) [3, 5, 7]. Within this framework, trajectories starting from the same ground-state configuration may later diverge due to the topography of the PES, leading to different fission outcomes. This is illustrated for the fission of ^{236}U in Fig.1. However, the location and quantum-mechanical origin of these bifurcations are poorly understood [3, 8–12].

As the excitation energy of the fissioning system varies, new fission valleys on the PES may become accessible [6, 14, 15]. This makes excitation energy dependence of fission fragment properties a key observable to gain insight into the nature of bifurcations.

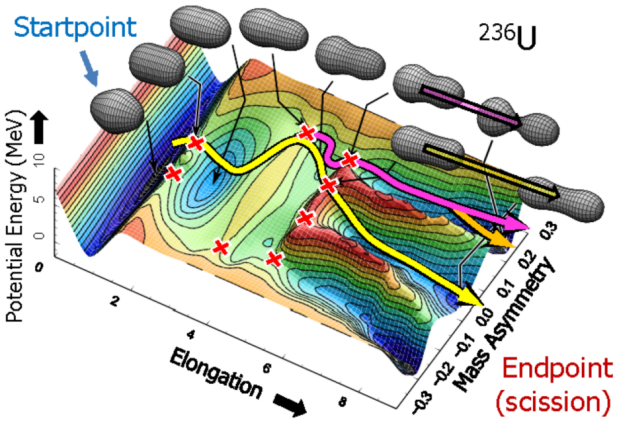

Figure 1. Potential energy surface of ^{236}U, adapted from Ref. [13]. The red crosses indicate saddle points, while the pink and orange lines on the PES show pathways to different fission modes.

Transfer-induced fission, in which a projectile nucleus transfers one or more nucleons, induces a continuous range of excitation energies below and above the fission barrier. By measuring the projectile-like fragment energy and angle, the excitation energy induced in the fissioning nucleus can be identified event-by-event, making transfer reactions ideal to study the excitation energy dependence of fission outcomes.

This paper presents the development of a new detector array for measurements of transfer induced fission at the Australian National University, and some preliminary results on the excitation energy dependence of fission fragment properties.

*e-mail: daniel.lee@anu.edu.au
**Present address: Laboratory of Ion Beam Physics, ETH Zürich, Switzerland

2 Experimental Details and Analysis

A continuous beam of 20.0 MeV deuterons with a beam current of 75 pnA was produced at the Heavy Ion Accelerator Facility (HIAF) at the Australian National University. The beam was delivered onto a target of ^{232}Th with an areal density of 131 μg/cm^2 oriented at 80° to the beam axis, with a aluminium backing of thickness 57 μg/cm^2 oriented downstream of the beam. The velocity of the fission fragments and protons from the (d,p) reactions is reduced by their traversal through the target materials and inactive materials in the detectors. This depends on the effective thickness of the materials, which varies with particle emission angle. Position-dependent energy loss corrections were applied event-by-event using stopping power calculations from Ziegler *et al.* [16].

Two detector arrays were combined for the current work. The outgoing protons from the transfer reaction ^{232}Th(d,p)^{233}Th were detected and characterised by ΔE-E$_{res}$ silicon detectors (the BALiN array [17]), while the binary fission fragments induced from the fission of ^{233}Th were detected using multi-wire proportional counters (CUBE fission spectrometer [18]) as described in detail in Sec. 2.1 and 2.2, respectively. A range of excitation energies up to ~13 MeV above the ground-state of ^{233}Th were populated in the transfer reaction.

2.1 Particle identification from the BALiN array

The Breakup Array for Light Nuclei (BALiN) [17] consists of four double-sided silicon strip detectors (DSSDs) arranged into two ΔE-E$_{res}$ telescopes each with thicknesses of 400 μm and 1500 μm for the ΔE and residual (E$_{res}$) layers respectively. The ΔE layer (MMM DSSD from Micron semiconductors Ltd.) is divided into 16 arcs (each 6.4 mm wide), and 8 sectors (each spanning 6.68° in the plane of the detector) as described in Ref. [17]. The E$_{res}$ layer (MMM5 DSSD from Micron semiconductors Ltd.) is divided into 15 arcs (each 6.4 mm wide), and 8 sectors (each spanning 6.84°). A 101.8 μm aluminium foil was placed in front of the ΔE layer to stop fission fragments while allowing lighter charged particles to pass through, preventing damage to the detectors from the intense fission fragments. Each ΔE-E$_{res}$ telescope measures the total energy (corrected for the energy loss through the aluminium foil), time of flight, and the angle of the charge particle going through the array.

To measure protons over a wide range of scattered angles (θ) from the (d,p) reaction, one ΔE-E telescope was placed at forward angles ($34° \leq \theta \leq 80°$) while the other was placed at backward angles ($100° \leq \theta \leq 157°$) with respect to the beam direction.

The ΔE-E$_{res}$ spectrum of particles measured in BALiN is shown in Fig. 2, where protons, deuterons and tritons are clearly separated. In the ΔE − E$_{res}$ spectrum, flat 'fold-back' features are observed which connect to the highest energy protons and deuterons in the E$_{res}$ detector. These features arise from incomplete energy deposition by charged particles in the DSSDs, where the particles have

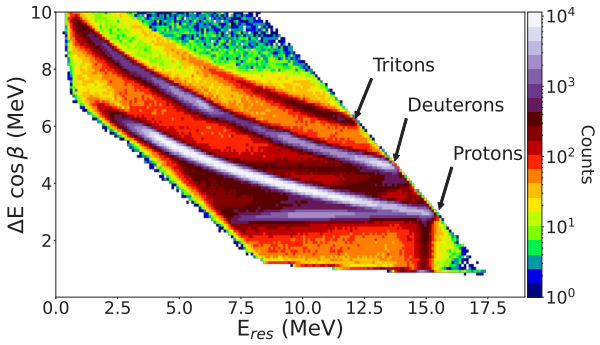

Figure 2. ΔE-E$_{res}$ particle identification spectrum measured in BALiN. A cosβ factor, where β is the angle of the particle from the unit normal vector to the DSSD face is multiplied to account for the difference in energy loss due to the different path lengths of the particle trajectories in the DSSD. The protons, deuterons and tritons are identified through their energy loss relationship [19], and are indicated.

sufficiently high energy to no longer fully stop in the residual layer. Such events with incomplete energy deposition were excluded from the analysis process.

The fission probability can be deduced from the ratio of the exclusive proton-fission coincidence yield to the inclusive proton singles yield. Proton singles were recorded with a trigger in BALiN, with a downscale factor of 100 due to their high count rate.

2.2 Measurement of fission fragment properties from the CUBE spectrometer

The configuration of CUBE for these measurements consists of two large multi-wire proportional counters (MWPCs) each with an active area of 279.0 mm × 357.0 mm, with the normal vectors to the detector facing laboratory angles of 45° and 135°. The fission fragments were measured in coincidence (one on each MWPC), and the centre of mass velocities of the fission fragments were reconstructed via the kinematic coincidence method [20]. The mass ratio of the fission fragments is defined as

$$M_R = \frac{m_1}{m_1 + m_2} = \frac{v_{cm,2}}{v_{cm,1} + v_{cm,2}}, \quad (1)$$

where m_i and $v_{cm,i}$ are the mass and the centre of mass velocity of the binary fission fragments. The masses of fission fragments were obtained directly from the mass of the fissioning compound nucleus, while their charges were derived from the charge of the fissioning compound nucleus, assuming the unchanged charge density approximation [21].

2.3 Timing correlations of protons with fission fragments

In this experiment a continuous beam was used to minimise the instantaneous rate, and hence rate of spurious coincidences between protons and fission fragments. However, some random coincidences of protons and fission

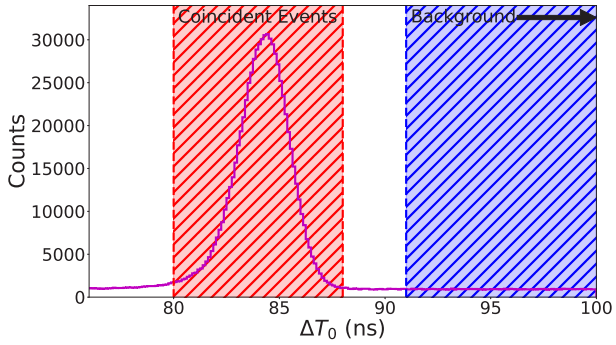

Figure 3. Difference in the times at which the beam nucleus interacted with the target nucleus, as deduced from proton arrival times in BALiN and fission fragment arrival times in CUBE. The red shaded region corresponds to the true coincidence window selecting protons in coincidence with fission fragments, while the blue shaded region indicates the region of spurious coincidences between protons and fission fragments used for background subtraction.

fragments remain. To identify true coincidences between protons and fission fragments, the time at which the beam nucleus interacted with the target nucleus (T_0) was deduced from the measured arrival time of both the fission fragments in CUBE ($T_{0,FF}$), and the protons in BALiN ($T_{0,p}$):

$$T_{0,i} = T_{det,i} - ToF_i, \quad (2)$$

where for a particle type i, $T_{det,i}$ is the time of arrival of the particle at its respective detector, and ToF_i is the time of flight deduced from the known flight path length and velocity of the particle. The proton velocities were derived from the measured energies in BALiN, while the fission fragment velocities were inferred using the time difference method [22], which enforces an average kinetic energy dependence as a function of the mass ratio of the fission fragments [6]. The times at which beam nucleus interacts with the target nucleus as deduced from BALiN and CUBE should coincide for a single (d,p) event, where the difference in these times ($\Delta T_0 = T_{0,FF} - T_{0,p}$) show a peak of coincident event in Fig. 3.

A peak with a FWHM of 3.2 ns is observed in the red shaded region, corresponding to events where the protons are in coincidence with the fission fragments. The arbitrary offset of ~84 ns arises from the time differences in the electronic processing of BALiN and CUBE. A small constant background of spurious coincidences of protons and fission fragments is present, so a background subtraction was performed. Due to the low background yield, data from a background region five times the width of the true coincident window were used to determine the background rate. Events belonging to the background region were time-shifted to match the coincidence window, processed identically to the true coincidence events normalised, and subtracted bin-by-bin from the coincidence data to obtain the background-subtracted plots of fission fragment properties, as shown in Fig. 4.

Following this step, the proton times were used as a reference for fission timings, allowing the fission fragment velocities to be reconstructed via the kinematic coincidence method [20]. This avoids assumptions about the total kinetic energy and allows reconstruction of individual fission fragment velocities, event-by-event.

2.4 Excitation energy reconstruction

The excitation energy, E^*, of the fissioning compound nucleus from the (d,p) reaction were obtained by

$$E^* = E_d + Q_{gg} - E_p - E_r, \quad (3)$$

where E_d is the incident deuteron energy in the centre of mass frame corrected for energy loss through the target, Q_{gg} is the ground-state to ground-state Q-value, and E_p, E_r are the kinetic energies (energy loss corrected) of the proton and the recoiling target-like nucleus, respectively. Each of these quantities are either known, measured, or deduced from two-body kinematics, allowing the excitation energy of the ^{233}Th nucleus to be deduced event-by-event.

The calculated excitation energies from the experiment span a continuous range (5.5 – 13 MeV above the ground-state energy), with an estimated resolution of ~75 keV.

3 Results

The reconstructed fission fragment mass distributions are shown in Fig. 4, as a function of excitation energy. They display a clear dependence on the excitation energy of the fissioning system. At excitation energies just above the fission barrier, indicated by the red long-dashed line [23], the distribution is dominated by mass asymmetric fission, with the heavy fragment centred near Z~54 and A~140. Above 9 MeV of excitation energy, an increase of symmetric fission yield (at around $M_R = 0.5$) begins to be observed, with the ratio of yields of symmetric to asymmetric fission gradually increasing with excitation energy, in agreement with previous results [6]. This is consistent with the expectation that the shell effects driving mass asymmetric fission begin to be attenuated with increasing excitation energy, while the symmetric mode does not exhibit a rapid dependence on the change in excitation energy. Above 10.5 MeV of excitation energy, there is a further increase in the fission fragment yields, due to the onset of second-chance fission. In this region, fission fragments from ^{233}Th and ^{232}Th are present due to competing decay channels of fission and neutron evaporation following the fission of ^{233}Th.

The evolution of the mean M_R of heavy fission fragments (in the region $0.56 \leq M_R \leq 0.65$) with excitation energy is shown in Fig. 5. The average mass of the heavy fragment shifts closer towards the standard I mode ($M_R \approx 0.58$ [4]) with increasing excitation energy until about ~10 MeV. It then moves towards the standard II mode ($M_R \approx 0.62$ [4]) before moving back towards the standard I mode again. A similar periodic shift in the mass is observed in fission of ^{233}Pa for $E^* \geq 12$ MeV in Ref. [6], which was interpreted in terms of competition of standard I and II modes, and contributions from multi-chance fission. The increase in M_R centroid towards standard II

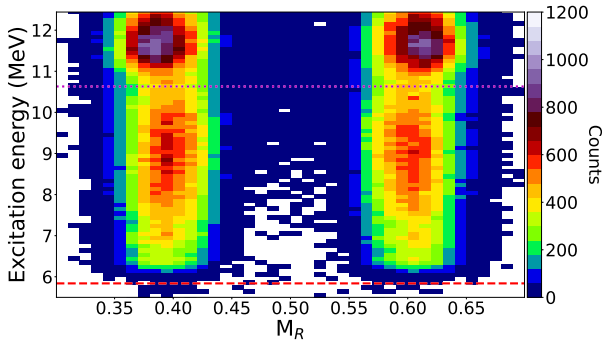

Figure 4. The mass distribution of fragments formed from fission of ^{233}Th as a function of excitation energy of the system. The red long-dashed line indicate the location of the fission barrier at $E^* = 5.84$ MeV [23]. The purple dotted line indicates the excitation energy corresponding to the one neutron separation energy above the fission barrier.

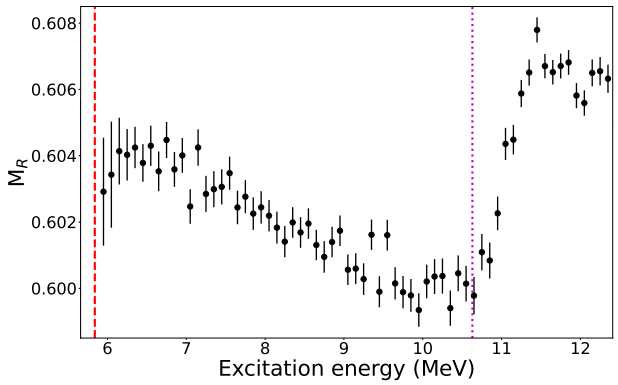

Figure 5. Evolution of centroid of the fission fragment mass distribution of the heavy asymmetric fragment with excitation energy, for fission of ^{233}Th. The red dashed line indicates the location of the fission barrier of ^{233}Th, while the purple dotted line indicates the excitation energy corresponding to the one neutron separation energy above the fission barrier. The error bars shown are given by $\sqrt{N}$ in each mass bin, where N is the number of counts in that bin.

mode can be attributed to the onset of second chance fission, with the threshold energy at $E^* = 10.8$ MeV indicated by the purple dotted line. To correctly reconstruct the fission fragment masses from the admixture of fission of ^{233}Th and ^{232}Th in this region, the fission probabilities for multi-chance fission must be extracted and accounted for.

In the region below the purple dotted line where no contribution from multi-chance fission is expected, there is a shift in the average mass of the heavy fragment. One possible interpretation for this initial shift towards the standard I mode is the excitation energy dependence of relative yields of the standard I and II modes of fission [3], naively assuming the width of the gaussian-like modes remain approximately constant over the excitation energy range. Other interpretations that involve changes in the topography of the PES with excitation energy [3, 24] may be possible, but the evolution of the mass centroid as a function of excitation energy clearly demonstrates an excitation energy dependence of the fission modes in actinides. This may inform theoretical descriptions of nuclear fission and its applications.

4 Conclusions

Two independent detector systems were successfully combined to enable surrogate (d,p) fission measurements at the Australian National University, designed to detect how fission fragment properties evolve with excitation energies close to the fission barrier. Some preliminary results on the excitation energy dependence of fission fragment mass distribution of ^{233}Th were discussed. Further work is in progress to reconstruct other fission fragment properties such as the total kinetic energy, fission probability and angular anisotropy, which are expected to depend on the excitation energy of the fissioning system [25–27]. Systematic comparisons with fission of the other actinides (^{235}U, ^{238}U, ^{244}Pu, ^{245}Am and ^{248}Cm) have been measured using the detector systems and methodology presented in this work, and will be the subject of a further publication.

Acknowledgements

This work was supported by Australian Research Council Grants DP200100601, DE230100197, DP230101028 and DP250101791. The authors acknowledge the facilities, and the scientific and technical assistance provided by Heavy Ion Accelerators (HIA). HIA is supported by the Australian Government through the National Collaborative Research Infrastructure Strategy (NCRIS) program. Discussions with Cédric Simenel regarding the excitation energy dependence of fission modes are gratefully acknowledged. S.L.H., H.L., T.T. and M.M.W. acknowledges support from the Australian Government Research Training Program (RTP) Scholarship.

References

[1] A. Chatillon, J. Taïeb, H. Alvarez-Pol, L. Audouin, Y. Ayyad, G. Bélier, J. Benlliure, G. Boutoux, M. Caamaño, E. Casarejos et al., Experimental study of nuclear fission along the thorium isotopic chain: From asymmetric to symmetric fission, Phys. Rev. C **99**, 054628 (2019). 10.1103/PhysRevC.99.054628

[2] G. Scamps, C. Simenel, Impact of pear-shaped fission fragments on mass-asymmetric fission in actinides, Nature **564**, 382–385 (2018). 10.1038/s41586-018-0780-0

[3] U. Brosa, S. Grossmann, A. Müller, Nuclear scission, Phys. Rep. **197**, 167–262 (1990). 10.1016/0370-1573(90)90114-H

[4] C. Böckstiegel, S. Steinhäuser, K.H. Schmidt, H.G. Clerc, A. Grewe, A. Heinz, M. de Jong, A.R. Junghans, J. Müller, B. Voss, Nuclear-fission studies with relativistic secondary beams: Analysis of fission channels, Nucl. Phys. A **802**, 12–25 (2008). 10.1016/j.nuclphysa.2008.01.012

[5] C. Simenel, A.S. Umar, Heavy-ion collisions and fission dynamics with the time-dependent hartree–fock theory and its extensions, Prog. Part. Nucl. Phys. **103**, 19–66 (2018). 10.1016/j.ppnp.2018.07.002

[6] A.C. Berriman, D.J. Hinde, D.Y. Jeung, M. Dasgupta, H. Haba, T. Tanaka, K. Banerjee, T. Banerjee, L.T. Bezzina, J. Buete et al., Energy dependence of p+^{232}Th fission mass distributions: Mass-asymmetric standard I and standard II modes, and multichance fission, Phys. Rev. C **105**, 064614 (2022). 10.1103/PhysRevC.105.064614

[7] P. Möller, D.G. Madland, A.J. Sierk, A. Iwamoto, Nuclear fission modes and fragment mass asymmetries in a five-dimensional deformation space, Nature **409**, 785–790 (2001). 10.1038/35057204

[8] K. Mazurek, C. Schmitt, J.P. Wieleczko, P.N. Nadtochy, G. Ademard, Critical insight into the influence of the potential energy surface on fission dynamics, Phys. Rev. C **84**, 014610 (2011). 10.1103/PhysRevC.84.014610

[9] A. Zdeb, M. Warda, L.M. Robledo, Description of the multidimensional potential-energy surface in fission of ^{252}Cf and ^{258}No, Phys. Rev. C **104**, 014610 (2021). 10.1103/PhysRevC.104.014610

[10] Z. Matheson, S.A. Giuliani, W. Nazarewicz, J. Sadhukhan, N. Schunck, Cluster radioactivity of $^{294}_{118}$Og$_{176}$, Phys. Rev. C **99**, 041304 (2019). 10.1103/PhysRevC.99.041304

[11] J. Randrup, P. Möller, Brownian shape motion on five-dimensional potential-energy surfaces:nuclear fission-fragment mass distributions, Phys. Rev. Lett. **106**, 132503 (2011). 10.1103/PhysRevLett.106.132503

[12] A. Bulgac, P. Magierski, K.J. Roche, I. Stetcu, Induced fission of ^{240}Pu within a real-time microscopic framework, Phys. Rev. Lett. **116**, 122504 (2016). 10.1103/PhysRevLett.116.122504

[13] A.N. Andreyev, K. Nishio, K.H. Schmidt, Nuclear fission: a review of experimental advances and phenomenology, Rep. Prog. Phys. **81**, 016301 (2018). 10.1088/1361-6633/aa82eb

[14] J. Randrup, P. Möller, Energy dependence of fission-fragment mass distributions from strongly damped shape evolution, Phys. Rev. C **88**, 064606 (2013). 10.1103/PhysRevC.88.064606

[15] K. Shimada, C. Ishizuka, F.A. Ivanyuk, S. Chiba, Dependence of total kinetic energy of fission fragments on the excitation energy of fissioning systems, Phys. Rev. C **104**, 054609 (2021). 10.1103/PhysRevC.104.054609

[16] J.F. Ziegler, M.D. Ziegler, J.P. Biersack, SRIM – The stopping and range of ions in matter (2010), Nucl. Instrum. Methods Phys. Res. B **268**, 1818–1823 (2010). https://doi.org/10.1016/j.nimb.2010.02.091

[17] R. Rafiei, R.d. Rietz, D.H. Luong, D.J. Hinde, M. Dasgupta, M. Evers, A. Diaz-Torres, Mechanisms and systematics of breakup in reactions of ^{9}Be at near-barrier energies, Phys. Rev. C **81**, 024601 (2010). 10.1103/PhysRevC.81.024601

[18] T. Banerjee, D.J. Hinde, D.Y. Jeung, K. Banerjee, M. Dasgupta, A.C. Berriman, L.T. Bezzina, H.M. Albers, C.E. Düllmann, J. Khuyagbaatar et al., Systematic evidence for quasifission in ^{9}Be–, ^{12}C–, and ^{16}O-induced reactions forming ^{258,260}No, Phys. Rev. C **102**, 024603 (2020). 10.1103/PhysRevC.102.024603

[19] H. Bethe, Zur Theorie des Durchgangs schneller Korpuskularstrahlen durch Materie, Ann. Phys. (Berlin) **397**, 325–400 (1930). 10.1002/andp.19303970303

[20] D.J. Hinde, M. Dasgupta, J.R. Leigh, J.C. Mein, C.R. Morton, J.O. Newton, H. Timmers, Conclusive evidence for the influence of nuclear orientation on quasifission, Phys. Rev. C **53**, 1290–1300 (1996). 10.1103/PhysRevC.53.1290

[21] A.C. Wahl, R.L. Ferguson, D.R. Nethaway, D.E. Troutner, K. Wolfsberg, Nuclear-charge distribution in low-energy fission, Phys. Rev. **126**, 1112–1127 (1962). 10.1103/PhysRev.126.1112

[22] B.M.A. Swinton-Bland, M.A. Stoyer, A.C. Berriman, D.J. Hinde, C. Simenel, J. Buete, T. Tanaka, K. Banerjee, L.T. Bezzina, I.P. Carter et al., Mass-asymmetric fission of ^{205,207,209}Bi at energies close to the fission barrier using proton bombardment of ^{204,206,208}Pb, Phys. Rev. C **102**, 054611 (2020). 10.1103/PhysRevC.102.054611

[23] K.H. Schmidt, B. Jurado, C. Amouroux, C. Schmitt, General description of fission observables: GEF model code, Nucl. Data Sheets **131**, 107–221 (2016). 10.1016/j.nds.2015.12.009

[24] P. McGlynn, C. Simenel, Extraction of fission mode properties from fragment mass distributions, Phys. Rev. C **111**, 034619 (2025). 10.1103/PhysRevC.111.034619

[25] J. Blons, A third minimum in the fission barrier, Nucl. Phys. A **502**, 121–140 (1989). 10.1016/0375-9474(89)90658-1

[26] V. Geppert-Kleinrath, F. Tovesson, J.S. Barrett, N.S. Bowden, J. Bundgaard, R.J. Casperson, D.A. Cebra, T. Classen, M. Cunningham, D.L. Duke et al. (NIFFTE Collaboration 2), Fission fragment angular anisotropy in neutron-induced fission of ^{235}U measured with a time projection chamber, Phys. Rev. C **99**, 064619 (2019). 10.1103/PhysRevC.99.064619

[27] A. Parihari, S. Santra, A. Pal, N.L. Singh, K. Mahata, B.K. Nayak, R. Tripathi, K. Ramachandran, P.K. Rath, R. Chakrabarti et al., Fission fragment angular distributions in ^{6,7}Li +^{235,238}U reactions, Phys. Rev. C **90**, 014603 (2014). 10.1103/PhysRevC.90.014603